NTU Journal for Renewable Energy (2025)Vol.9 (1):12-22
DOI: https://doi.org/10.000000/ntujre.v9 i1

IRAQI Academic Scientific Journals

EISSN: 2788-9920
NTU Journal for Renewable Energy
Available online at:
https://journals.ntu.edu.iq/index.php/NTU-JRE

Investigation of the Impact of Utilizing Lauric Acid and Paraffin Wax as PCM in a Single - Pass Solar Air Heater: Experimental Study

Yahya Yousif Yahya[1], Ahmed Mustaffa Saleem[1]

[1]Northern Technical University, Engineering Technical College of Mosul, Cultural Group Street, Mosul, Iraq

Article Information

Received: 27 – 03 - 2025
Accepted: 05 – 07 - 2022
Published: 15 – 07 - 2025

Corresponding Author:
Yahya Yousif Yahya

Email:
yahya_yosif@ntu.edu.iq

Key words:
Air Heater, Improved Solar Air Heater, Lauric Acid, paraffin Wax, Phase Change Material, Traditional Solar.

ABSTRACT

This current investigation involved an experimental inspection of adding Lauric acid (LA) above the absorber surface of solar air heater (SAH) in comparison with SAH integrated with paraffin wax and traditional SAH to evaluate the thermal performance of the SAH. To assess the efficacy of adding LA, all three SAHs operate under identical operating conditions. In the improved SAH model, LA is positioned above the absorber plate, and paraffin wax is incorporated above the absorber plate, whereas the conventional SAH model depicts the standard configuration. Data was gathered in Mosul City, Iraq, for January 18 and February 12, 25, 2025, with experiments performed at a constant air mass flow rate of 0.02223 kg/s. The findings confirms that the thermal performance of improved LA SAH is better than enhanced paraffin wax SAH and traditional SAH by 7.4% and 102% for January 18, and by 8.9% and 93.9% for February 12, and by 8.96% and 97.5% for February 25 respectively. The traditional SAH model records efficiency of 84%, 82%, and 83.5%, for 18 Jan, 12 and 25 Feb., respectively. The findings indicate a substantial maximum temperature differential attained by the enhanced SAH model utilizing (LA) and paraffin wax in comparison to the conventional SAH model.

Introduction

Solar thermal systems constitute the primary classification of solar energy systems. Various types of solar collectors have been developed in recent years, with solar air heaters (SAHs) being often utilized. These thermal systems encompass a broad spectrum of low to moderate-temperature applications, including drying, cooking, and air-conditioning systems [1]. Renewable energy is considered an efficient method to mitigate the detrimental impacts of climate change and the exhaustion of fossil fuel resources. Solar power has attracted considerable attention as a renewable energy source due to its abundant availability and sustainability. However, additional challenges remain, including the variability of solar energy due to climatic conditions, the significant costs associated with the initial installation and maintenance of solar systems, and the requirement for efficient energy storage solutions to ensure a dependable power supply. Moreover, the integration of solar energy into existing energy systems presents technological and regulatory challenges that must be addressed to ensure reliability and efficiency [2]. The utilization of solar air heaters (SAHs) for the production of heated air in industrial applications is a significant application of solar energy. Hot air is utilized to provide comfortable air conditioning in cold areas and to eliminate moisture from goods including chemicals, vegetables, lumber, bagasse, and aquatic products. The principal disadvantages of SAH include its diminished heat transfer rates with air as the working fluid, heightened heat losses to the environment at elevated operating temperatures, and inconsistent availability of solar radiation [3-5]. Solar power has attracted considerable attention as a renewable energy source due to its abundant availability and sustainability. Solar air heaters are categorized into glazed and unglazed variants. Glazed collectors possess glass cover plates that facilitate solar transmission while reducing heat loss, demonstrating great efficiency. **Yassmin, et al**. [6] conducted an investigation into the thermal performance of solar air collectors featuring wavy and corrugated absorbers, comparing them to traditional flat absorbers under equivalent climatic conditions in Sfax, Tunisia. Their experimental findings revealed notable enhancements in thermal efficiency, with wavy absorbers exhibiting a 22.89% increase and corrugated absorbers achieving a 40.56% improvement. Regarding daily exergy efficiency, the corrugated absorber demonstrated a 44.83% rise, while the wavy absorber recorded a 23.24% enhancement. Furthermore, when evaluating cost-effectiveness and reductions in CO_2 emissions, the corrugated absorber emerged as the most advantageous choice, highlighting the significance of absorber design in optimizing energy efficiency and promoting environmental sustainability. **Şevik and Abuşka** [7] conducted an assessment of the thermal efficiency of a SAH that utilized a single-pass semi-flexible foil duct as its absorber, without any alterations to the surface. Their experiments, which were carried out at air mass flow rates of 0.013 kg/s and 0.03 kg/s, as well as under conditions of natural convection, revealed that the semi-flexible duct attained a peak thermal efficiency of 65.48% and an average efficacy of 53.08% at the flow rate of 0.03 kg/s. This represented an 18.82% enhancement compared to traditional flat plate absorbers. Additionally, the innovative design exhibited an exergy efficiency ranging from 10% to 15%, and its heat transfer coefficient was found to be 2.03 times greater than that of the flat plate configuration. Furthermore, the Nusselt number for the new heater was increased by a factor of 3.02. **Omojaro and Aldabbagh** [8] investigated the thermal performance of single and double pass solar air heaters with attached fins and a steel wire mesh absorber. The effects of air mass flow rates (0.012 kg/s to 0.038 kg/s) on outlet temperature and thermal efficiency were analyzed, with bed heights of 7 cm and 3 cm for the lower and upper channels, respectively. Results indicated that efficiency improved with increasing air mass flow rate. The double pass heater demonstrated 7–19.4% higher efficiency than the single pass at the same flow rate, achieving maximum efficiencies of 59.62% and 63.74% respectively at 0.038 kg/s. Additionally, increasing the height of the first pass in the double pass heater led to decreased thermal efficiency, and the outlet-ambient temperature difference diminished as flow rates rose.. **A.S. Abdullah et al.** [9] experimentally examined the impact of adding turbulators and external mirrors to a single pass SAH to enhance its efficiency. Aluminum cans were utilized as turbulators, and external mirrors improved the energy input. Three designs of absorbing plates were tested: a flat plate without cans, a flat plate with cans in an aligned arrangement, and a flat plate with cans in a staggered arrangement. The study compared the performance of modified SAHs with and without reflectors to conventional SAHs, utilizing air mass flow rates ranging from 0.02 to 0.05 kg/s. The results indicated that the staggered heater with external reflectors and guide vanes achieved a maximum daily efficiency of approximately 73.4% at 0.05 kg/s. **SatyenderSingh et al.**[10] examined an experimental configuration of a double pass converging finned wire mesh packed bed SAH. This design incorporates two distinct air channels: the upper channel situated between the glass cover and the absorber plate, and the lower channel located between the absorber and the back plates. The inclusion of two glass covers serves to reduce thermal losses, while the converging fins improve convective heat transfer by expanding the heat exchange surface area and increasing air velocity. Sixteen fins, positioned at an angle of 11°, form periodic converging sections, and ten layers of wire

mesh ensure high porosity and effective thermal energy storage. The solar air heater demonstrates a peak thermal efficiency of 93% and a thermohydraulic efficiency of 80% at specific flow rates, with optimal performance yielding hot air at 55°C under designated solar radiation conditions. **Kumar et al.** [11] conducted an analysis of an enhanced SAH that incorporates a V-corrugated absorber plate and utilizes shot-blasting technology on its internal surface. Performance evaluations at airflow rates ranging from 0.01 to 0.02 kg/sec indicated that the modified SAH attained an energy efficiency improvement of 15% and an exergy efficiency increase of 34% compared to the traditional SAH at the 0.02 kg/sec rate. Furthermore, the research encompasses an assessment of the environmental impact and sustainability of the SAH. **Rui Fan, et al.** [12] discussed the solar hot air heating system that utilizes evacuated tube collectors (ETCs) integrated with phase change materials (PCM), emphasizing its efficacy in plateau regions. They developed and validated a model using TRNSYS software, which was subsequently employed in a comparative analysis of the energy efficiency of six different solar heating systems, including fully electric options, tailored for various building types in Lhasa. The results indicate that the solar hot air heating system is particularly suitable for plateau environments, providing nighttime heating and requiring less maintenance. Additionally, the study investigates the impact of several factors, such as collector area and buffer tank volume, on the system's performance, which will inform future designs and applications for winter heating in these regions.. **Soliman and Cheng.** [13] assessed the thermal efficiency of a traditional solar collector (TSC) in comparison to a proposed solar collector (PSC) that incorporates PCM and rectangular ducting. The PSC is equipped with three rectangular ducts, one of which contains paraffin wax as the PCM, facilitating prolonged energy storage and enhanced water heating. Additionally, the design features a partitioned water duct that optimizes fluid flow. A comprehensive evaluation encompassing energy, exergy, economic factors, and environmental implications revealed that the PSC significantly surpassed the TSC, achieving a 19.6% increase in the average outlet water temperature and a 35.34% enhancement in useful energy attributable to the integration of PCM. **Wadhawan et al.** [14] developed a SAH that utilizes Lauric acid as PCM to improve thermal energy storage capabilities. They conducted experiments to evaluate the performance of the heater both with and without the thermal energy storage device (TESD). The findings indicated that the increase in output air temperature diminished from 8.67 K to 4 K as the air mass flow rate increased from 0.021 kg/s to 0.035 kg/s. Furthermore, the friction factor was observed to decrease from 0.0119 to 0.00802 with the rise in mass flow rate. The implementation of the TESD led to an average enhancement of 86.47% in output air temperature and a 36.47% rise in the friction factor when compared to the configuration without TESD. **González-Peña, et al,** [15] introduced an innovative design for photovoltaic and thermal (PV/T) technology that features thermal storage, integrating a PCM tank positioned at the rear of the PV panel. This configuration not only optimizes thermal energy storage but also enhances the efficiency of the PV panel by regulating temperature during the phase change process. Furthermore, the inclusion of a black surface perimeter surrounding the panel increases thermal energy absorption. Testing a prototype that utilized lauric acid as the PCM in two different configurations resulted in an overall daily efficiency of 50%, which has the potential to be improved through effective management of the PCM temperature throughout the day. **Mohammed and Saleem** [16] this study aims to design, build, and assess the SAH's performance with an integrated enhanced PCM absorber storage system. Using materials found locally, two single-pass solar air heaters were designed and produced for this study. **Srivastava et al.**[17] considered the application of lauric acid as a PCM for the storage of surplus solar energy in a solar drying process, emphasizing heat transfer properties during the charging and discharging phases. The study analyzed the influence of inlet hot air temperature and velocity on charge duration, as well as the effect of ambient air velocity on discharge duration. **Salah , et, al** [18] the study evaluated the thermal efficiency of a double-pass solar air heater (DP-SAH) using rectangular capsules filled with paraffin wax as a phase change material (PCM). It involved computational and experimental assessments during charging and discharging operations, utilizing an artificial sunshine simulator for indoor testing. The system was tested at three solar irradiation levels (625, 725, and 825 W/m2) and various airflow speeds (0.6 to 1.8 kg/min). Results showed that higher airflow velocities reduced the melting point of paraffin and extended the duration of the melting process. Lauric acid (LA) is an advantageous phase change material (PCM) for thermal energy storage owing to its beneficial thermal and physical characteristics. A principal characteristic of LA is its elevated latent heat capacity, enabling it to store and release substantial quantities of thermal energy during phase transitions, thereby rendering it appropriate for diverse thermal management applications, including electronic cooling and building energy efficiency [19,20].

The present study aims to compare the performance of three solar air heater (SAH) systems: the first is a traditional SAH, the second SAH is integrated with paraffin wax as PCM, and the third SAH is integrated with lauric acid as PCM. Our findings indicate that lauric acid is a more effective phase change material (PCM)

than paraffin wax, with the conventional compound following in efficiency. The efficiencies of the improved LA SAH on 18 January and 12 , 25 February 2025, was 159%, 157%, and 160.5% respectively, whereas the efficiencies of paraffin wax as PCM was 148%, 145%, and 145.5%. The efficiencies of the traditional SAH on the aforementioned dates was 84%, 82%, and 83.5% respectively.

1. Experimental work

1.1. Experimental setup design and construction

Figure 1 illustrates the pictorial and schematic photo of traditional and improved SAHs. three collectors featuring an aluminum frame filled with foam, characterized by inner dimensions measuring (1.16 x 0.76) m and outer dimensions of (1.20 x 0.8) m, with a plate thickness of 1 mm. The first model called Traditional SAH and the tow modified collectors called Improved SAH integrated with Lauric acid (LA) and paraffin wax as PCM. The existing models operates as a single-glazed system, maintaining a vertical clearance of 7.5 cm above the absorber. The glass has a thickness of 6 mm.LA and Paraffin wax fourteen tubes each, PCM is filled inside individual tubes with filling ratio of 85%, [23]. The tubes are characterized by a thickness of approximately 1 mm, an inner diameter of 13.6 mm, and an outer diameter of 15.6 mm. The inlet ports of three SAHs configurations are outfitted with four fans with adjustable speed to ensure adequate air circulation within the proposed system.

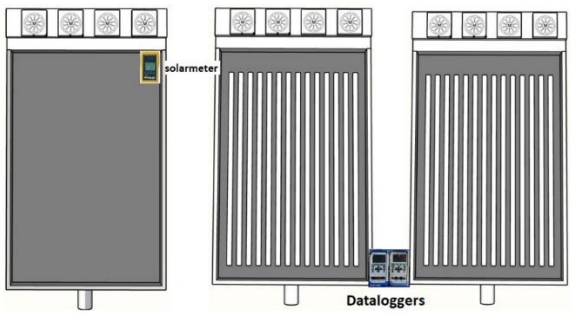

Fig 1 schematic view of Traditional and tow Improved SAHs (Lauric acid and Paraffin)

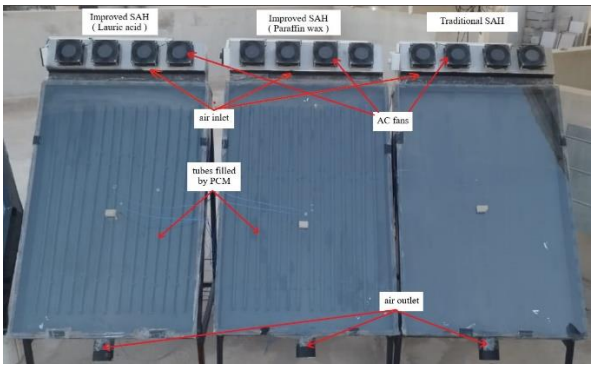

Fig. 2. pictorial photo for three SAH collectors

1.2. Physical characteristics of Lauric Acid

Table I illustrates the physical and thermal properties of the commercial LA employed in this study. Each tubes contain 100 grams of LA as PCM. To ensure safety, To alleviate the pressure on the tubes, lauric acid was filled by 85% of the total tube volume. Initially, the liquid alloy is heated to transition it into a liquid phase, followed by the filling of the tubes to guarantee uniform distribution. Figure 3 illustrates the current condition of the material of LA.

Table I. Physical Characteristics of LA.[24]

Physical properties of Lauric acid		
Properties of Lauric acid	Unit	value
Milting temperature ($T_{L)}$	ºC	48.2
Solidification temperature ($T_{s)}$	ºC	43.5
Latent heat (L_H)	kJ/kg	187.21
Specific heat capacity of solid (CP_S)	kJ/kg K	2.18
Specific heat capacity of liquid (CP_L)	kJ/(kg K	2.39
Density solid (ρ_S)	kg/m^3	940
Density liquid (ρ_L)	kg/m^3	885
thermal conductivity of solid (K_S)	W/m K	0.16
Thermal conductivity of liquid (K_L)	W/m K	0.14
Volume expansion	%	15%

Fig. 3. Lauric acid material with purity 99%

1.3. Physical characteristics of Paraffin Wax

Table II illustrates the physical and thermal properties of the commercial Paraffin wax employed in this study. The tubes contain 100 grams of Paraffin wax as the PCM per tube. To ensure safety, 85% of the tubes' volume is occupied by LA to mitigate pressure on the tubes. Initially, the liquid alloy is heated to transition it into a liquid phase, followed by the filling of the tubes to guarantee uniform distribution. Figure 4 illustrates the current condition of the material of Paraffin wax.

Table II. Physical Characteristics of Paraffin wax [17,25]

Physical properties of Paraffin Wax		
Properties of Paraffin wax	Unit	value
Milting temperature ($T_{L)}$)	ºC	58-60
Solidification temperature ($T_{s)}$)	ºC	43.5
Latent heat (L_H)	kJ/kg	187.21
Specific heat capacity of solid (CP_S)	kJ/kg K	1.85
Specific heat capacity of liquid (CP_L)	kJ/(kg K	2.38
Density solid (ρ_S)	kg/m^3	880
Density liquid (ρ_L)	kg/m^3	760
thermal conductivity of solid (K_S)	W/m K	0.2
Thermal conductivity of liquid (K_L)	W/m K	0.4
Volume expansion	%	12.5%

Fig. 4. Paraffin wax material

2. Experimental procedure

Several thermocouples are employed to measure temperature fluctuations within the integrated SAH. These sensors quantify multiple factors, including intake and exit temperatures, as well as airflow. Figure 5 illustrates a schematic depiction of three systems, indicating the positions of thermocouple sensors.

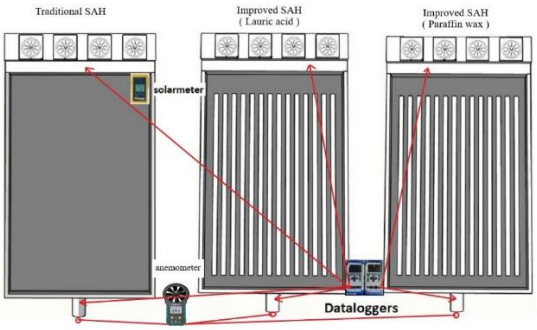

Fig. 5. Schematic view of three systems illustrated the distribution of thermocouples

To achieve a precise comparison, the intake and output temperatures of three systems are assessed under identical weather conditions to elucidate the effects of utilizing LA and paraffin wax as phase change materials (PCM). The experiments are performed at a constant mass flow rate of 0.02223 kg/s. The glass covers are cleaned prior to commencing the testing, and all equipment is inspected to confirm the absence of leaks at any joints. Three models have comparable size and a slope angle of 55º relative to the horizontal. The solar radiation and temperatures at the intake and outflow are recorded during tests conducted from 9 AM to 8 PM. Solar radiation is quantified using a solar meter (Seaward Solar Survey 100 Irradiance Meter) with an accuracy of ±0.85 W/m². A multi-channel thermocouple with an accuracy of ±0.2°C is employed to measure the temperatures of different components of solar collectors. A detailed representation utilizing precision and accuracy of instruments is provided in Table III. The standard uncertainty is determined using the following equation [22].

$$u = \frac{a}{\sqrt{3}} \qquad (1)$$

where (a) is the device accuracy

Table III. Specifications of equipment sensor devices.

Measurement instrument	Specification	Accuracy	Standard uncertainty
Anemometer (MT-4615)	AP- 816B	0.01 m/s	0.0058 m/s
Thermocouples	k-type (10 in number)	± 0.2°C	0.115°C
Solar power meter	Seaward SS200R	± 0.85 W/m^2	0.491 W/m^2
Indicator of temperature	8,2 channels data logger	--	--

The current experiments were conducted in Mosul, Iraq (latitude 36.410108° N and longitude 43.112963° E), utilizing three locally made solar air heaters of identical dimensions. The initial model is the traditional (SAH), the second model is an enhanced SAH including paraffin wax as a phase change material (PCM), and the third model is an improved SAH utilizing (LA) as a PCM. The three models are positioned southward at an inclination angle of 55º relative to the horizontal plane. To maintain a consistent air mass flow rate of 0.02223 kg/s for both the Traditional and Improved SAH, four fans were employed. The experiments were conducted on January 18 and from February 12 to 25, 2025. The data was gathered and documented, encompassing the intake temperature, exit temperature, and ambient temperature. Thermodynamics and thermal efficiency were subsequently computed utilizing this data.

3. Solar Air Heater Thermal Performance Calculations.

In the current investigation the useful energy and the thermal performance has been calculated as follows [7,18]:

$$Q_u = m \cdot * C_p * \Delta T \quad (2)$$

The thermal performance of the SAH collector (ηth) can be obtained as the ratio of useful energy to the solar energy that reached the aperture area [5]:

$$Qi = I * Ac \quad (3)$$

and:

$$\eta_{th} = \frac{Qu}{Qi} \quad (4)$$

Where :
Q_u = Useful energy
$m.$ = Mass flowrate
C_p = specific heat
ΔT = temperature difference
I = solar radiation

The mass flow rate of the air (ṁ) through the collectors can be calculated by using the following equation [17]:

$$\dot{m} = \rho\ air * At * Vair \quad (5)$$

Therefore, the thermal efficiency of a SAH can be determined using the following formula [14]:

$$\eta\ th = m * Cp * (Tout - Tin) * I * Ac \quad (6)$$

where: ρ = air density
At = Total area
Vair = air velocity
Tout = outlet temperature
Tin = intake temperature
Ac = area of the collector

4. Results and Discussion

Figure 6 illustrates a comparative analysis of solar radiation intensity (W/m²) over three days: January 18th, February 12th, and February 25th. The line graph shows diurnal variations in solar irradiance from 9:00 AM to 5:30 PM, revealing a parabolic trend typical of the daily solar cycle. February 25th, marked by a blue line, peaks at approximately 980 W/m² around 12:30 PM, indicating optimal solar conditions. February 12th (red line) follows closely with a peak of about 920 W/m², while January 18th (square markers) has the lowest peak at 850 W/m². Initial solar radiation values at 9:00 AM were around 380, 450, and 650 W/m² for the respective days. By 5:30 PM, all values drop below 100 W/m². The curves overlap during peak hours, suggesting stable solar irradiance conditions, with February 25th showing slightly better performance. These insights are crucial for optimizing solar energy system design and performance predictions.

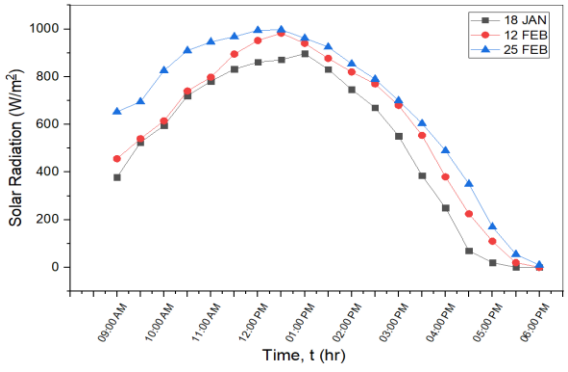

Fig. 6. Variations in the intensity of solar radiation on 18 JAN and 12 - 25 FEB 2025

Figure 7 illustrates the diurnal variation of ambient temperature (°C) over three days: January 18th, February 12th, and February 25th. The line graph compares these temperatures, revealing a parabolic trend typical of daily cycles. February 12th shows the highest temperatures, peaking at 19.5°C, while January 18th follows with a peak of 17.5°C. In contrast, February 25th exhibits much lower temperatures, peaking at only 8.5°C. This variation is crucial for understanding the performance of temperature-sensitive systems, such as solar collectors, as the higher temperatures on February 12th could reduce efficiency due to smaller temperature differences with the environment. The distinct temperature profiles underscore the importance of considering ambient conditions when analyzing experimental results, as they significantly influence heat transfer rates and system efficiency.

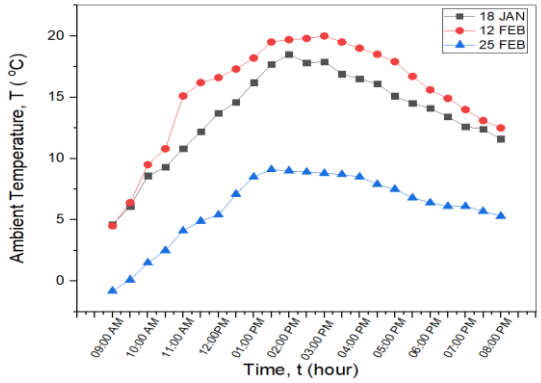

Fig. 7. Ambient temperature variation on 18 JAN and 12 - 25 FEB 2025

Figure 8 illustrates a comparative analysis of the differential temperature (ΔT) for a traditional SAH across specific dates: January 18th, February 12th, and February 25th. The ΔT quantifies the temperature difference between the collector's outlet and inlet, the temperature difference between the collector's outlet and inlet. Notably, on February 12th, ΔT reaches its maximum at approximately 31 °C at 1:30 PM, signifying ideal operational conditions. In contrast, January 18th records lower ΔT values, peaking at about 27 °C at 12:30 PM. On February 25th, the peak ΔT is around 30 °C at 12:00 PM. The fluctuations in ΔT are influenced by environmental variables such as solar irradiance and ambient temperature, with a marked decrease in ΔT occurring as solar input diminishes, which is in contrast to collectors that incorporate PCM.

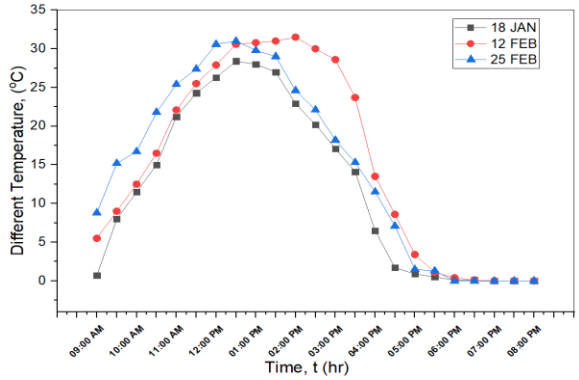

Fig. 8. Shows temperature differences for the traditional SAH system.

Figure 9 illustrates the useful energy (Qu) output of a traditional SAH over three days: January 18th, February 12th, and February 25th, measured in watts (W) from 9:00 AM to 8:00 PM. The line graph shows a parabolic trend for each day, indicating the collector's performance is influenced by solar irradiance. February 25th achieves the highest output of approximately 675 W at noon, starting from 160 W at 9:00 AM and declining to 20 W by 6:00 PM. February 12th peaks at 650 W at 1:00 PM, beginning at 150 W and also reaching 18 W by 8:00 PM. January 18th starts at 20 W, peaks at 590 W at 1:30 PM, and falls to 20 W by 8:00 PM. The variations in output highlight the collector's dependence on environmental factors like solar irradiance, ambient temperature, and wind speed. The data serve as a baseline for comparing enhanced collector designs with thermal storage capabilities.

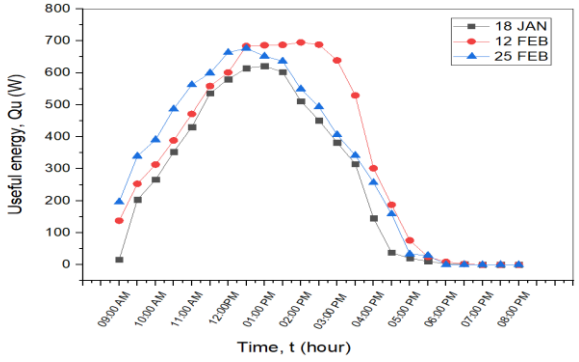

Fig. 9. illustrated the useful energy for traditional SAH system

Figure 10 illustrates a comparative analysis of the differential temperature (ΔT) in degrees Celsius of a thermal energy storage system using paraffin wax as a PCM. The ΔT values, plotted over three days (January 18th, February 12th, and February 25th), represent the difference between outlet and inlet temperatures. On

February 12th, indicated by a red line markers, ΔT starts at 9°C at 9:00 AM, peaks at around 30°C at 1:30 PM, and declines to 1.5°C by 8:00 PM, demonstrating effective heat absorption. January 18th, represented by a black line, shows a lower peak of approximately 25°C at 2:00 PM, starting from 0.5°C at 9:00 AM and declining to 0.5°C by 8:00 PM. February 25th, shown by a blue line, exhibits the lowest ΔT, beginning at 5°C, peaking at 28°C at 12:30 PM, and decreasing to around 2°C by 8:00 PM. The variations in ΔT highlight the system's sensitivity to external factors, with peak values correlating with solar irradiance. Overall, the data confirm that the paraffin wax effectively absorbs and releases heat, providing insights into its thermal behavior under real-world conditions.

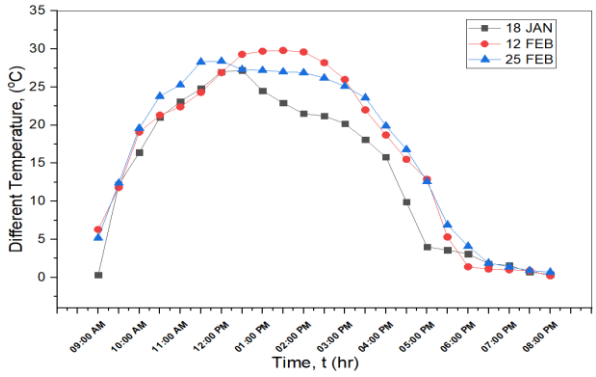

Fig. 10. Variation in different temperature throughout experimental days for improved SAH(by using paraffin wax)

Figure 11 illustrates the temporal profile of useful energy (Qu) in watts for a thermal energy system using paraffin wax as a PCM, across three days: January 18th, February 12th, and February 25th. The line graph shows time on the x-axis and useful energy on the y-axis, allowing for comparative analysis of energy performance under varying environmental conditions. The data reveals a parabolic trend, influenced by diurnal solar irradiance. February 12th shows the highest output, peaking at approximately 670 W at 1:00 PM, while January 18th peaks at 600 W and February 25th reaches nearly 610 W. The curves indicate a strong correlation between solar irradiance and energy output, with variations suggesting differences in system efficiency or external factors like temperature and solar intensity. Overall, the data is crucial for optimizing paraffin wax systems in thermal energy applications, demonstrating sensitivity to environmental changes.

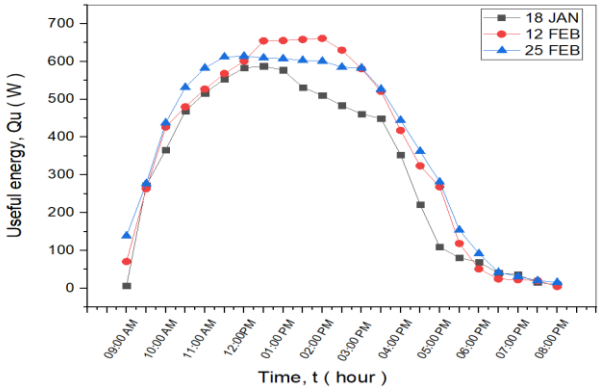

Fig. 11. illustrated the useful energy for Improved SAH (by using paraffin wax)

Figure 12 illustrates a comparative analysis of the differential temperature (ΔT) of a system using lauric acid as a phase change material for thermal energy storage, measured over three days (Jan 18th, 12th, and 25th FEB). On February 12th, the highest ΔT peaks at approximately 34.5°C at 1:00 PM, starting from 9°C at 9:00 AM and declining to 2°C by 8:00 PM, indicating effective heat absorption during high solar irradiance. January 18th shows a lower peak of 28°C at 1:30 PM, starting from 1°C, and ending at 2.5°C by 8:00 PM, suggesting less favorable conditions for temperature differences. February 25th records the lowest ΔT, peaking at 29°C at 12:30 PM, starting from 7°C and dropping to 3°C by 8:00 PM, indicating less intense solar irradiance or higher heat losses. The variations in ΔT across the three days highlight the system's sensitivity to external factors, with peak values correlating with solar irradiance. Despite differences in magnitude, all days demonstrate significant ΔT, confirming lauric acid's effectiveness in heat absorption and release.

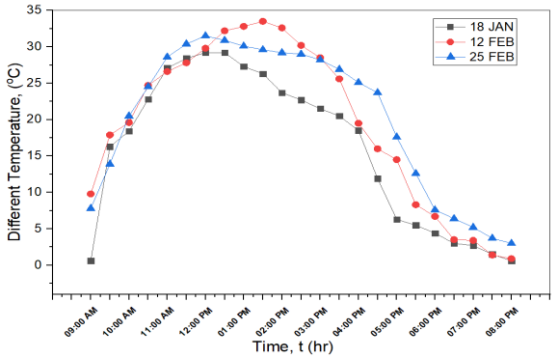

Fig. 12. Variation in different temperature throughout experimental days for improved SAH (by using Lauric acid)

Figure 13 illustrates the temporal profile of useful energy (Qu) in watts (W) for a system using lauric acid as a PCM over three days: January 18th, February 12th, and February 25th. The curves, generally parabolic, reflect the influence of solar irradiance variations. On February 12th (red line), Qu starts at about 200 W at 9:00 AM, peaks at 750 W around 1:00 PM, and declines to 25 W by 8:00 PM, indicating optimal energy collection likely due to high solar irradiance and favorable temperatures. February 25th (blue line) shows a similar trend with a lower peak of nearly 690 W at 12:30 PM, starting at 150 W and ending at 55 W by 8:00 PM, suggesting reduced energy performance. In contrast, January 18th (black line) begins close to 0 W, peaks at 600 W at 1:30 PM, and drops to 30 W by 8:00 PM, indicating lower energy output possibly due to lower solar irradiance or less favorable conditions. The parabolic curves suggest a correlation between solar irradiance and energy output, while variations in peak values highlight differences in system efficiency across the days.

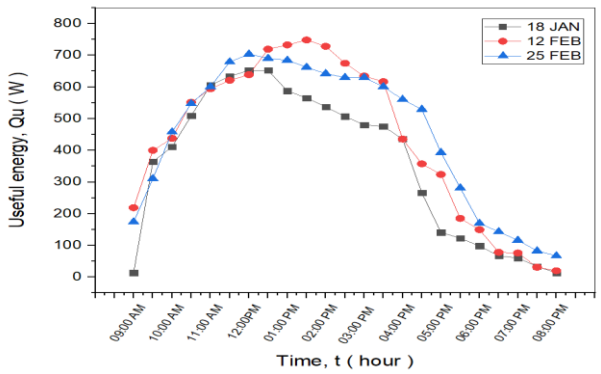

Fig. 13. shows the useful energy Qu curve for improved SAH (by using Lauric acid)

Figure 14-15-16 compares the thermal efficiency of three SAH collector designs: one with lauric acid as a PCM, one with paraffin wax as a PCM, and a traditional collector without PCM.

Figure 14 illustrates the data gathered on January 18th. The efficiency curves deviate from the conventional bell-shaped pattern, with certain values surpassing 100%, which suggests the presence of thermal storage. Between 9:00 AM and 3:00 PM, the performance of both PCM collectors is comparable, with LA exhibiting a slightly ahead. However, post 3:00 PM, the paraffin collector demonstrates the highest efficiency. The LA collector begins at 0% efficiency at 9:00 AM, climbs to approximately 85% by noon, and reaches a peak of nearly 159% by 5:00 PM. Similarly, the paraffin wax collector shows a comparable trajectory, achieving 82% by noon and around 148% by 5:00 PM. In contrast, the traditional collector starts at 0% and peaks at 84% by 12:30 PM, but experiences a sharp decline to 0% by 4:30 PM.

Figure 15 presents data collected on February 12th, illustrating thermal efficiency. The efficiency curves exhibit an atypical pattern, with certain values exceeding 100%, which suggests the presence of thermal storage. The paraffin wax collector begins with an efficiency of 40%, rises to 82% by 12:30 PM, exceeds 100% around 2:45 PM, and ultimately reaches a maximum of nearly 145% by 5:00 PM. In contrast, the LA collector demonstrates a generally higher trend, with efficiencies surpassing 100% at approximately 3:15 PM and achieving 157% by 5:00 PM. The traditional collector starts at 22% efficiency, peaks at 82% by 12:30 PM, but experiences a significant decline, dropping to nearly 0% by 5:00 PM.

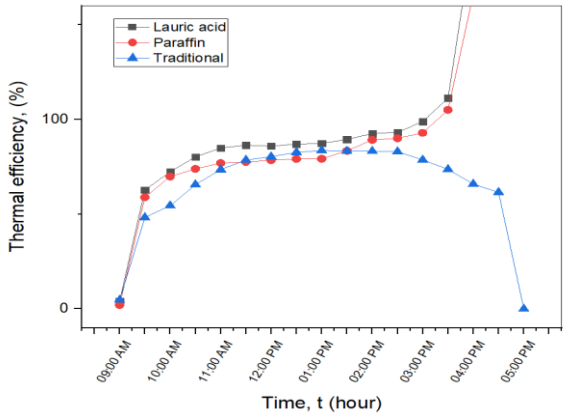

Fig. 14. shows thermal performance of 3 SAHs in 18 January

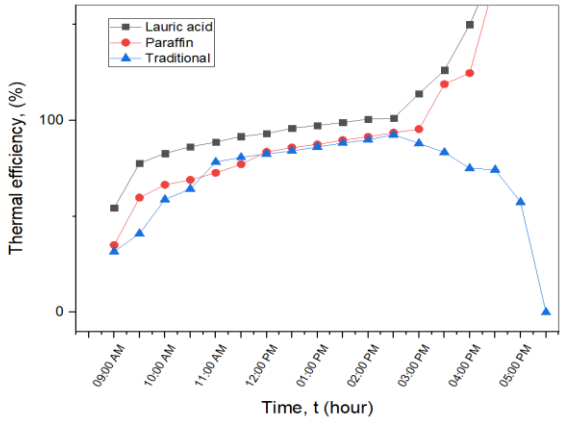

Fig. 15. shows thermal performance of 3 SAHs in 12 February

Figure 16 presents data gathered on February 25th. The efficiencies of the PCMs collectors demonstrate a progressive increase throughout the day, surpassing 100%, which indicates their capacity for thermal storage. The paraffin wax collector begins with an efficiency of 35% and achieves a maximum of nearly 146.5% by 5

PM. In contrast, the lauric acid collector starts at 38% and reaches approximately 160.5% at the same time. The traditional collector, which initiates at around 22%, peaks at 83.5% but experiences a rapid decline to 0% by 5 PM. These findings highlight the benefits of PCM technology, with LA exhibiting superior performance compared to paraffin wax, thereby underscoring the critical role of thermal storage in improving overall efficiency.

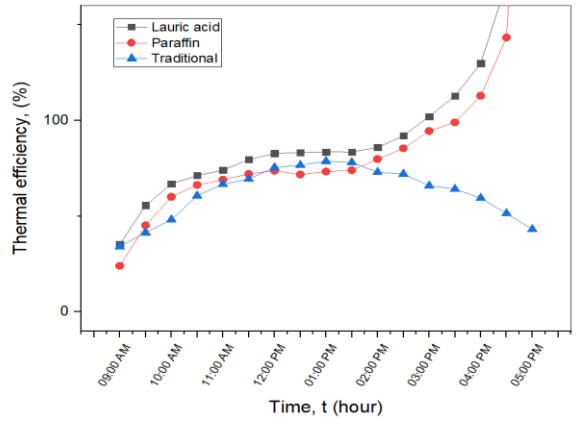

Fig. 16. shows thermal performance of 3 SAHs in 25 February

Conclusion

An experimental study was conducted to evaluate the thermal performance of the SAH, specifically to display the effect of adding LA as a phase change material on the absorber plate, comparing it with a SAH combined with paraffin wax and a conventional SAH. To confirm the effect of adding LA on the absorber plate, the performance of improved SAH integrated with LA is compared with enhanced SAH integrated with paraffin wax and traditional SAH under same operation conditions. The three systems were designed with identical dimensions and surface areas. The experiments were conducted in January and February 2025 in Mosul, Iraq. The results of this research yielded several noteworthy observations.

1. The results indicate that the thermal efficiency of the improved SAH model surpasses that of the enhanced SAH and traditional SAH for all testing days.

2. The highest efficacy of the improved SAH was 159% for January 18 and 157% for February 12 and was 160.5% for February 25.

3. The findings confirms that the thermal performance of improved LA SAH is better than enhanced paraffin wax SAH and traditional SAH by 7.4% and 102% for January 18, and by 8.9% and 93.9% for February 12, and by 8.96% and 97.5% for February 25 respectively.

4. As the ambient temperature increase the temperature difference between intake and outlet from the system decrease

5. The results indicated that the integrating LA and paraffin wax with SAH enhance the thermal performance of the system

6. The improvement observed in the performance of the improved SAH system indicates that the utilization of LA significantly influences both heat exchange and the rate of heat transfer.

References

[1] S. A. Gandjali khan Nassab, (2025), A High-performance Double-pass Solar Air-water Heater, Iranica Journal of Energy and Environment, vol (16), 353-363. http://**doi**: 10.5829/ijee.2025.16.02.15

[2] Sharol, A. F., Razak, A., Majid, Z. a. A., Azmi, M. a. A., Tarminzi, M., Ming, Y., Zakaria, Z., Harun, M. A., Fazlizan, A., & Sopian, K, (2022), Effect of thermal energy storage material on double-pass solar air heater performance with cross-matrix absorber, Journal of Energy Storage, vol (51), 104494. https://doi.org/10.1016/j.est.2022.104494

[3] Abhishek Saxena , Varun , A.A. El-Sebaii, (2015), A thermodynamic review of solar air heaters, Renewable and Sustainable Energy Reviews, vol (43), 863 – 890. http://dx.doi.org/10.1016/j.rser.2014.11.059

[4] Ehsan Hasan Zaim , Hadi Farzan, "Effects of PCM Mass on Heat Dynamics and Thermal Performance of Solar Air Heaters: A Numerical and Analytical Study, (2021), Journal of Renewable Energy and Environment, vol (8), 45 – 53. https://doi.org/10.30501/jree.2021.259570.1169

[5] A.K.Srivastava, S.K.Shukla and Sandeep Mishra, (2014) , Evaluation of Solar Dryer/Air Heater Performance and the Accuracy of the Result, Energy Procedia vol (57),2360 – 2369. https://doi.org/10.1016/j.egypro.2014.10.244

[6] Yassmin Touhami, Ridha Boudhiaf, Abd Elnaby Kabeel, Abdelkrim Khelifa, Mohammed El Hadi Attia, Moataz M. Abdel-Aziz, Noureddine Latrache, Abederrahmane Aissa,Zied Driss, (2024), Effect of absorber shape on energy, exergy efficiency and enviro-economic analysis of solar air collector: An experimental study, Environmental Progress & Sustainable Energy, vol (43), 14481. http://doi: 10.1002/ep.14481

[7] Seyfi Şevik, Mesut Abuşka, (2020), Enhancing the thermal performance of a solar air heater by using single-pass semi-flexible foil ducts, Applied Thermal Engineering. vol (179), 115746. https://doi.org/10.1016/j.applthermaleng.2020.115746

[8] A.P. Omojaro, L.B.Y. Aldabbagh , (2010), Experimental performance of single and double pass solar

air heater with fins and steel wire mesh as absorber, Applied Energy, (87), 3759–3765.
http://doi:10.1016/j.apenergy.2010.06.020

[9] A.S. Abdullah, M.I. Amro, M.M. Younes, Z.M. Omara, A.E. Kabeel, F.A. Essa, (2020) Experimental investigation of single pass solar air heater with reflectors and turbulators, Alexandria Engineering Journal, (59), 579–587.
https://doi.org/10.1016/j.aej.2020.02.004

[10] Satyender Singh, Laxmikant Dhruw, Subhash Chander, (2019), Experimental investigation of a double pass converging finned wire mesh packed bed solar air heater, Energy Storage, vol (21), 713–723.
https://doi.org/10.1016/j.est.2019.01.003

[11] Satyender Singh, Prashant Dhiman, (2016) Thermal performance of double pass packed bed solar air heaters – A comprehensive review, Renewable and Sustainable Energy Reviews, vol (53), 1010–1031.
http://dx.doi.org/10.1016/j.rser.2015.09.058

[12] Rui Fan, Yue Li, Ting Bu, Kexin Sun, Yibing Zhou, Jie Shi, Xinyu Zhang, (2020), Comparative study of solar hot air heating systems with phase change materials in plateau areas", Energy & Buildings, vol (224), 110265.
https://doi.org/10.1016/j.enbuild.2020.110265

[13] Ahmed Saad Soliman, Ping Cheng, (2025), 4E analysis of a flat plate solar collector using phase change material and rectangular channels , Applied Thermal Engineering (265),125641-125655.

[14] Amol Wadhawan, A.S. Dhoble, V.B. Gawande, (2018), Analysis of the effects of use of thermal energy storage device (TESD) in solar air heater, Alexandria Engineering Journal, (57), 1173-1183.
http://dx.doi.org/10.1016/j.aej.2017.03.016

[16] David González-Peña, Iván Alonso-deMiguel, Montserrat Díez-Mediavilla, Cristina Alonso-Tristán, (2020), Experimental Analysis of a Novel PV/T Panel with PCM and Heat Pipes, sustainability journal,vol (12), 1710.
http://doi:10.3390/su12051710

[17] Zeina Ahmed Mohammed, Ahmed Mustaffa Saleem, (2024), Investigation of the impact of utilizing PCM into a coil in a single-pass air heater (experimental study)", NTU Journal for Renewable Energy, vol (7), 98-106.
https://doi.org/10.56286/ntujre.v7i1

[18] Salah M. Salih, Jalal M. Jalil, Saleh E. Najim, (2019), Experimental and numerical analysis of double-pass solar air heater utilizing multiple capsules PCM, Renewable Energy, vol (143), 1053-1066.
http://dx.doi.org/10.1016/j.aej.2017.03.016

[19] Osama Khan, Ibrahim Alsaduni, Mohd Parvez, Zeinebou Yahya, Ashok Kumar Yadav, (2024) , Role of hydrogen-enrichment on performance and emission characteristics of a diesel engine fuelled with metal oxide nanoparticles added biodiesel/diesel blends:A combined neuro Fuzzy-Gaussian Mixture Model analysis , International Journal of Hydrogen Energy, vol (93), 1113-1126.
https://doi.org/10.1016/j.ijhydene.2024.11.032

[20] Mohammed A. Basim, Omar Rafae Alomar, (2024) , Impacts of Adding Porous Media and Phase Change Material on Performance of Solar Water Distiller System Under Iraq Climatic Condition: An Experimental Study, Energy Storage vol(6),1-15.
https://doi.org/10.1002/est2.70038

[21] Burak Markal, Kubra Aksoy, (2021), The combined effects of filling ratio and inclination angle on thermal performance of a closed loop pulsating heat pipe, Heat and Mass Transfer, vol (57), 1-13.
https://doi.org/10.1007/s00231-020-02988-6

[22] Bin Huang, Lin-Li Tian, Qing-Hua Yu, Xun Liu, Zu-Guo Shen, (2021) , Numerical Analysis of Melting Process in a Rectangular Enclosure with Different Fin Locations, energies, vol (14), 1-17.
https://doi.org/10.3390/en14144091

[23] P Bharadwaj Reddy,C Gunasekar,Atul Shalikrao Mhaske,Mr N Vijay Krishna, (ICAME 2018), Enhancement of thermal conductivity of PCM using filler graphite powder materials, IOP CONFERENCE SERIES: Materials Science and Engineering, pp. 1 – 10.
http://doi:10.1088/1757-899X/402/1/012173